Soft Matter

PAPER

View Article Online
View Journal | View Issue

Cite this: *Soft Matter*, 2025, **21**, 2915

How to estimate the surface coverage of polymer grafted planar substrates and spherical nanoparticles

Cheng-Wu Li, *[a] Holger Merlitz [a] and Jens-Uwe Sommer [ab]

Received 3rd January 2025,
Accepted 21st March 2025

DOI: 10.1039/d5sm00005j

rsc.li/soft-matter-journal

Surface coverage is an important parameter in describing the kinetics of adsorption in interface science, the adsorption theory of macromolecules (*e.g.*, proteins, DNA) on biomaterial surface, the stability of colloids with surface modifications and the application of surfactants at interfaces. In this work, we focus on nanoparticles (NPs) with polymer coatings and, with a mean-field approach, propose a universal theoretical model for calculating the coverage of polymers on planar or spherical substrates at different solvent qualities. Validated by molecular dynamics simulations, our model is applicable to a wide range of polymer morphologies – from partially occluded to completely covered NPs – and provides a novel quantitative approach to characterize this type of polymer patchy particles.

1 Introduction

Patchy particles, generated by a decoration with polymeric molecules, are a class of anisotropic colloids[1–4] with a variety of applications in biomedicine,[5] nanomaterials,[6] and interface science.[7] The fabrication of polymeric patchy particles can be achieved by attaching polymers in a "grafted-to" or "grafted-from"[8,9] manner to nanoparticles (NPs) with surface patterning,[10,11] such as "Janus" particles.[12] Another approach starts from a uniform polymer brush, where the surface pinned micelles are formed in response to changes in temperature or solvent quality.[13,14] Since the latter approach is reversible and the surface patches can be permanently preserved by a photo-crosslinking step, they can be designed as smart surfaces responding to external stimuli,[15] or to form self-assembled structures using these chemically distinct patches as covalents.[4,16–18] The realisation of these functions relies on the distinction between NPs and grafted polymers, in particular the transition from a uniform to a patchy coverage, which can be described by the degree of surface coverage. Since surface coverage plays an important role in adsorption kinetics,[19] biomolecule adsorption theory,[20] surfactant applications,[21] *etc.*, it is pre-controlled (such as surface-patterned NPs[22]) during fabrication. However, measuring the surface coverage of polymer patches that form through conformational transitions is rather challenging.

In good solvent, polymer chains grafted on a NP transform from isolated "mushrooms" to a semi-dilute brush of uniform thickness as the grafting density or chain length increases.[23] If the solvent quality drops subsequently, this brush layer may under certain conditions break up into varying numbers of pinned micelles (patches). This process is driven by the effective inter-monomer attraction and the reduction of the brush surface tension, as has been investigated in details in theory,[24–26] experiments[13,27,28] and simulations.[29–33] These works help to provide an understanding of planar brushes and isotropic spherical brushes in terms of spatial distribution, free energy and morphological transformations. However, for a polymer-induced anisotropy of an otherwise isotropic or symmetric NP, a general theory to depict the relative properties (polymer patches *versus* exposed NP substrate) as a function of the chain length, the grafting density and the size of the NP, is still lacking.

In this work, we characterise these anisotropic polymer patchy particles by defining the surface coverage and develop a universal theoretical model using a mean-field approach. The predictions of this model are then validated by the results of molecular dynamics (MD) simulations. The rest of this work is organized as follows: in Section 2, we introduce the MD simulation details and provide the definition of the surface coverage. A universal method for calculating the coverage of polymer coatings is presented for the first time. Using the mean-field approach for polymers in various morphologies, specific predictions and MD simulation results of the surface coverage for planar and spherical systems are presented in Sections 3 and 4, respectively. Finally, conclusions and discussions are summarised in Section 5.

[a] *Leibniz Institute of Polymer Research Dresden, 01069 Dresden, Germany. E-mail: chengwu-li@qq.com*
[b] *Institute for Theoretical Physics, TU Dresden, Zellescher Weg 13, Germany*

2 Simulation model and theoretical analysis of the surface coverage

2.1 MD simulation details

Using the open source LAMMPS software,[34,35] MD simulations of polymers decorated on planar and spherical NPs have been performed with a coarse grained bead-spring ('Kremer–Grest') model.[36] Pairwise interactions among monomers are delineated by the shifted Lennard-Jones (LJ) potential

$$U_{\mathrm{LJ}}(r) = 4\varepsilon[(d/r)^{12} - (d/r)^{6} - (d/r_{\mathrm{c}})^{12} + (d/r_{\mathrm{c}})^{6}], r \le r_{\mathrm{c}}, \quad (1)$$

where the depth of the potential ε is in energy unit of $k_{\mathrm{B}}T$. With the monomer-diameter d as the length unit, interactions are either truncated at the minimum for a fully repulsive force ($r_{\mathrm{c}} = \sqrt[6]{2}d$, implying an athermal solvent) or at longer ranges to account for attractive interactions ($r_{\mathrm{c}} = 2.5d$) and varying solvent qualities. The monomers are given a weak attraction of $\varepsilon = 0.5k_{\mathrm{B}}T$, at which the system temperature of $T = 1$ (dimensionless absolute temperature by the energy unit of $k_{\mathrm{B}}T$) corresponds to $2/3T_{\Theta}$, yielding a marginally poor solvent condition (with the longer cutoff) below the Θ-point.[37] A similar shifted LJ potential, with the cutoff at its minimum, is used to describe the interaction between monomers and the planar or spherical substrate ($\varepsilon = 0.5k_{\mathrm{B}}T$), creating a purely repulsive force that prevents the monomers from penetrating the substrate. Fully repulsive also implies a non-wetting substrate, whereas an attractive substrate would allow a wetting with the polymer phase.

The connectivity between bonded monomers is granted through a finite extensible nonlinear elastic (FENE) potential,[36]

$$U_{\mathrm{FENE}}(r) = -0.5KR_0^{2}\ln[1 - (r/R_0)^{2}] + U_{\mathrm{LJ}}(r) + \varepsilon \quad (2)$$

with a spring constant $K = 30\varepsilon/d^{2}$ and a maximum bond length of $R_0 = 1.5d$.

Once we summarise all free energy (eqn (1) and (2)) into a total potential of U_{tot}, the motion of the particles is described by the Langevin equation:

$$m\frac{\mathrm{d}^{2}\mathbf{r}_i}{\mathrm{d}t^{2}} + \zeta\frac{\mathrm{d}\mathbf{r}_i}{\mathrm{d}t} = -\frac{\partial U_{\mathrm{tot}}}{\partial \mathbf{r}_i} + \mathbf{F}_i, \quad (3)$$

where ζ represents the friction coefficient and is set as $\zeta = 1$. F_i is a Gaussian random force that was used to couple the system to the heat bath, satisfying the correlation function

$$\langle \mathbf{F}_i(t)\cdot\mathbf{F}_j(t')\rangle = 6k_{\mathrm{B}}T\zeta\delta_{ij}\delta(t - t'). \quad (4)$$

During the simulation with timestep of $\Delta t = 0.002\tau_0$, where τ_0 denotes the LJ time unit derived from the pure repulsive LJ potential (eqn (1)) to model the particles.[38]

To form a planar brush, we first define an impenetrable planar substrate in the xy-plane, and fix one end of 64 polymer chains with the same spacing to the same side of this plane. Periodic boundary conditions are applied in the extension (x–y direction) of the substrate, yielding an infinitely large planar brush with the grafting density σ (see Fig. 1(A)). By adjusting the chain length (polymerization N) and σ, we are able to simulate the planar system in various morphologies. In case of spherical NPs, we fix the diameter to $D = 40d$ and vary the number of grafted polymers to achieve the desired value for σ (see Fig. 1(B)). To ensure the equilibration of the systems, we first perform sufficient equilibration time steps (4×10^{7} to 1×10^{8} time steps, determined by approximately constant brush thickness and surface coverage), followed by an additional 4×10^{7} steps to collect the required data. For polymers grafted on a planar substrate, the grafting points are uniformly distributed with equal spacing of $\sigma^{-1/2}$. For polymers grafted on a spherical substrate, the grafting points are initially allowed to move freely on the sphere. A spontaneous uniform distribution of grafting points is achieved through 4×10^{7} steps of simulation under good solvent. Subsequently, these grafting points are fixed, and further simulations are carried out under both good and poor solvent conditions.

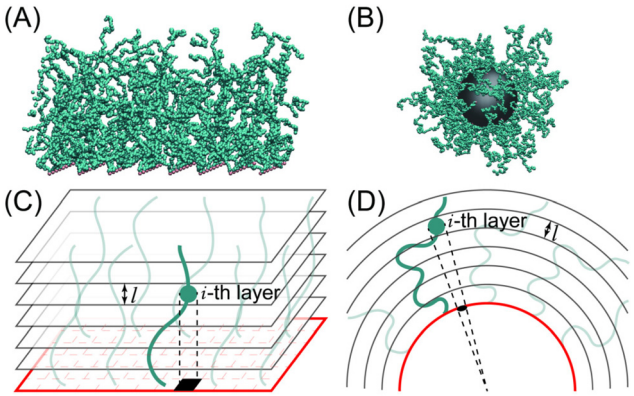

Fig. 1 Simulation snapshot and schematic illustration of polymers (green beads and lines) grafted onto (A), (C) planar and (B), (D) spherical NPs. In the sketches, brushes are uniformly divided into sublayers parallel to the substrate, with black shading indicating the normal projected area from the monomer (green bead) in i-th layer.

In the reduced units adopted in this work, $k_{\mathrm{B}}T$, the monomer diameter d, and the monomer mass m are defined as the units of energy, length, and mass, respectively, enabling the derivation of dimensionless forms for all parameters used herein. For example, the units of spherical diameter, grafting density, and number concentration can be dimensionlessied by $[D] = d$, $[\sigma] = d^{-2}$ and $[c] = d^{-3}$, respectively. In order to intuitively compare the dimensionless units with the practical units, we take the polystyrene with a molar mass of $M_0 = 104$ g mol^{-1} as an example. The chemical bond length between the monomers is about $a \approx 0.3$ nm (2 carbon–carbon bonds), and the persistence length is estimated as $L \approx 1$ nm.[39] Therefore, in MD simulations of the freely jointed chain model, the dimensionless units of energy, size, and mass correspond to $k_{\mathrm{B}}T \approx 4.14 \times 10^{-21}$ J (at $T \approx 300$ K), $d \approx 1$ nm, and $m = LM_0/\mathcal{N}_{\mathrm{A}}a \approx 5.76 \times 10^{-25}$ kg in practical units, respectively.

2.2 Definition and calculation of the surface coverage

The surface coverage (denoted by θ) indicates how much of the substrate is obscured by the polymers, and contributes not only

from monomers adsorbed on the surface, but also from those located above the substrate. Therefore, we define θ as the ratio of the normal projected area (black shading in Fig. 1(C) and (D)) of all monomers on the substrate to its total area. To achieve that, we divide the area of substrate into uniform lattices with the area of d^2 and then project the coordinates of all monomers onto these lattices. θ is calculated by recording the proportion of the number of lattice cells that are hit by the projections.

To derive a theoretical expression of θ, we start with the isotropic polymer brushes. Considering the shielding of monomers projected on the same surface lattice, we divide the brush (with the thickness H) into uniform sublayers (with the thickness l) parallel to the substrate as shown in Fig. 1(C) and (D). Then, the effective projected area of each monomer in the i-th layer on the substrate, the monomer number density, and the volume of the i-th layer can be represented by a_i, c_i and V_i, respectively. Theoretically, we can calculate the coverage of the i-th layer as $a_i c_i V_i/A$, where A is the substrate's area. By assuming that the coverage of the sublayers are statistically independent, we obtain the product

$$\theta = 1 - \prod_{i=1}^{H/l}\left(1 - \frac{a_i c_i V_i}{A}\right), \tag{5}$$

with the discretization length (the sublayer's thickness) l. The statistical independence assumption between sublayers is fundamentally rooted in the mean-field approximation, and therefore its validity must be verified through ensemble-averaged configurations. The accuracy of eqn (5) improves with decreasing l relative to the monomer diameter (in the order of Kuhn length in the simulations).

For anisotropic system of polymers (patches) on planar or spherical NPs, we follow the same "slicing" method, but calculate the coverages within each patch separately. For example, for the j-th patch with a vertical extension of R_j, the coverage of the patch over its own projected area S_j is obtained by replacing H and A in eqn (5) with R_j and S_j, respectively. Assuming P dispersed patches, the total surface coverage is computed as

$$\theta = \frac{1}{A}\sum_{j=1}^{P} S_j\left[1 - \prod_{i=1}^{R_j/l}\left(1 - \frac{a_{i,j}c_{i,j}V_{i,j}}{S_j}\right)\right], \tag{6}$$

where $a_{i,j}$, $c_{i,j}$ and $V_{i,j}$ stand for the effective single monomer projection area, the monomer number density, and the volume of the i-th sublayer inside the j-th patch, respectively. Since eqn (5) and (6) provide general expressions for θ, regardless of the substrate and solvent, we will next specify θ for planar and spherical cases in the next two sections depending to their morphology as well as the solvent quality.

3 Polymers on planar substrates

3.1 Theoretical analysis

We firstly investigate planar mushroom state case composed of M polymers, *i.e.*, each polymer chain containing N monomers with one end fixed on a plane forming a "mushroom"[40] of size R. We assume that these dispersed chains are identical and the monomers are uniformly distributed within each coil with a number density $c = N/R^3$, making the system equivalent to a plane with M identical polymer patches. By dividing the mushroom into sublayers of unity thickness ($l = d = 1$, d is the monomer diameter), the effective projected area of each monomer on the plane yields close to $d^2 = 1$, simplifying eqn (6) to

$$\theta = \frac{MS_j}{A}\left[1 - \left(1 - d^2 ch\right)^{R/l}\right] = \sigma S_j\left[1 - (1-c)^R\right], \tag{7}$$

where the projected area of each patch is $S_j \approx R^2$.

In good solvent, single-chain mushrooms are swollen with low number densities, and in the dilute limit ($c \to 0$), eqn (7) can be further simplified to

$$\theta \approx \sigma c R^3 \approx \sigma N. \tag{8}$$

As grafting density σ or N increase, the mushrooms grow until they reach overlap, at which point the layer forms a uniform surface brush,[41] being a semi-dilute brush with a porous structure, for which eqn (5) has to be applied. Taking the Alexander-deGennes[42,43] mean-field approach for the brush of height $H \sim \sigma^{1/3}N$, the scaling of the thickness of the sublayer as $l \equiv H/(\sigma^{1/3}N)$. Therefore, the number density of monomers is consistent in the number of $\sigma^{1/3}N$ sublayers as $c = \sigma^{2/3}/l$, yielding

$$\theta = 1 - (1 - a_{\mathrm{h}}\sigma^{2/3})^{\sigma 1/3N}, \tag{9}$$

where a_{h} represents the effective projected area from a monomer in the sublayer of the thickness l. Here we take a mathematical trick to eliminate H/l, since the assumption of density invariance (for semi-dilute brush) allows us to take any l without changing the calculation, which fails in the spherical geometry.

In poor solvent, again starting with polymers in the mushroom state, monomers in the single-chain mushroom are packed densely due to mutual attraction. Taking the condensed limit of $c \to 1$ in case of nonsolvent, the surface coverage with M mushroom patches (eqn (7)) simplifies to

$$\theta \approx \sigma R^2 \sim \sigma N^{2/3}, \tag{10}$$

with the mushroom size scaling as $R \sim N^{1/3}$. In contrast to good solvent, polymer chains in poor solvent tend to form patches due to the surface tension beyond the mushroom state. Here, we adopt the concept of octopus "micelle" proposed in William's work[25] to describe the formation of solvent-phobic patches from multiple polymer chains aggregation in poor solvent. At this point, those mushrooms grafted within a circular area of diameter R_{c} on the substrate will merge into a single octopus micelle with a diameter of R_{m}. They satisfy[25,30] $R_{\mathrm{m}} \sim \sigma^{1/5}N^{3/5}$ and $R_{\mathrm{c}} \sim \sigma^{-1/5}N^{2/5}$ respectively, leading to

$$\theta = R_m^2/R_c^2 \sim \sigma^{4/5}N^{2/5}. \quad (11)$$

Comparing eqn (10) and (11), the scaling behaviour of θ shifts at $\sigma \sim N^{-4/3}$, which is consistent with the condition at which polymers switch from the mushroom state to the micellar state.[25,30,41] Those micelles swell as σ and N increase, and eventually combine to form a uniform brush, accompanied by the limit of $\theta = 1$, a fully covered substrate.

3.2 Simulation results

Since eqn (8)–(11) illustrate the relationship between surface coverage θ and chain length N for planar substrate under various conditions, their accuracy can be validated through MD simulation results, as shown in Fig. 2. It is important to emphasize that when calculating surface coverage from simulation data, we do not employ the sublayer decomposition used in the theoretical analysis. Instead, we directly compute the projections of all monomers onto the substrate, regardless of their vertical positions. This approach inherently accounts for overlapping projections between different monomers, thereby automatically incorporating inter-layer correlation effects.

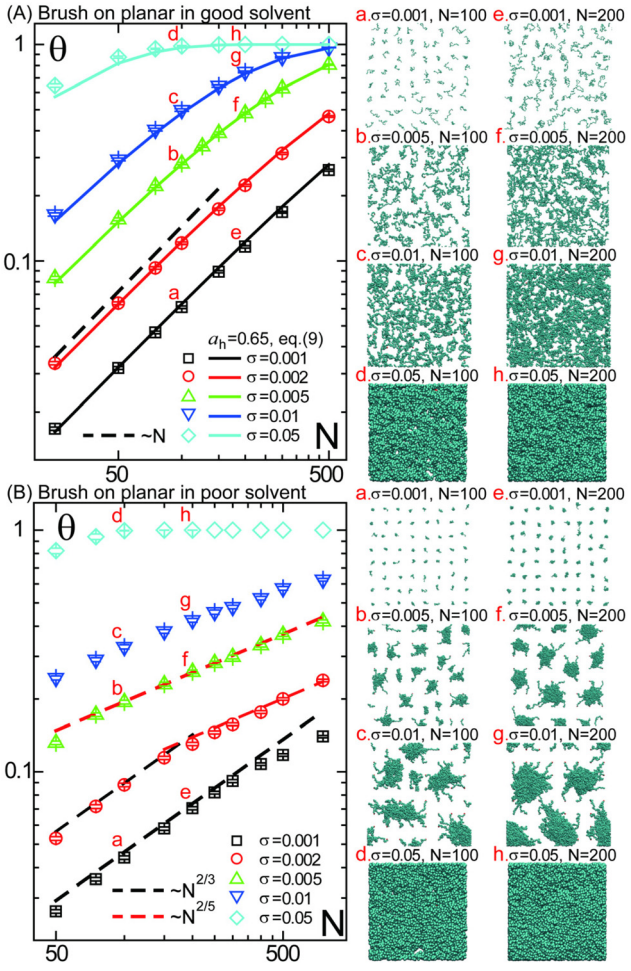

Fig. 2 Surface coverage θ of planar substrate as a function of polymerization N in (A) good and (B) poor solvent, at different grafting densities σ. Simulation snapshots of the top view are shown on the right, where the red markers (a)–(h) correspond to the labelled data points in the curves, respectively. The black and red dashed lines in (B) represent the scaling relations between θ and N predicted by eqn (10) and (11), respectively.

In good solvent (Fig. 2(A)), the linear relationship (eqn (8), black dashed line) only holds for short chains, at which dilute single chain patches dominate. Beyond the dilute regime, the predictions of θ *versus* N is governed by eqn (9), where a_h serves as a free parameter to fit the scaling prediction to the simulation results. Adopting a constant of $a_h = 0.65$, the theoretical predictions in Fig. 2(A) (solid lines, with different colours distinguishing the σ) show a high agreement with the simulation results (symbols). Additionally, although eqn (9) is derived for the semi-dilute brush, it can be approximated as $\theta \approx a_h\sigma N$ for smaller N and σ, reverting to the linear dependence characteristic of the mushroom regime (eqn (8)). This also explains why the predictions in of eqn (9) remain in good agreement with the coverage in the mushroom regime.

Fig. 2(B) illustrates θ *vs.* N under the poor solvent, at which the scaling prediction of $\theta \sim N^{2/3}$ (black dashed line, eqn (10)) is well satisfied within $\theta < 0.1$ (mushroom states in snapshots (a) and (e)). When $\theta > 0.1$, the scaling relationship shifts to $\theta \sim N^{2/5}$ (red dashed line, eqn (11)), implying the formation of micelles (snapshots (b), (c), (f), and (g)) which persist until complete coverage of the substrate is approached (snapshots (d) and (h)). Therefore, we can infer that the condensed limit assumption is roughly satisfied. Furthermore, in the case of $\sigma = 0.002$ (red-circled symbols), we can clearly distinguish the transition point ($N \approx 150$) in the scaling behavior of θ, which corresponds to the switch between the mushroom state and the micelle state.

The constant a_h in fitting the simulation data suggests that this parameter is insensitive to the chain length and grafting density in the semi-dilute brush regime. By converting eqn (9) into

$$\ln(1 - \theta) = \sigma^{1/3}\ln(1 - a_h\sigma^{2/3})N, \quad (12)$$

we can then rescale the simulation results onto a master curve. Therefore, $\ln(1 - \theta)$ is proportional to N, and the linear fitting slope consists the grafting density of polymers σ, and the effective projected area of a single monomer a_h.

Fig. 3(A) illustrates the relationship between $\ln(1 - \theta)$ and N and their linearly fitting curves (solid lines). According to the fitting slopes at different σ, we compute the relationship between a_h and σ as shown in the inset. We note that a_h tends to rise with increasing σ, but besides $\sigma = 0.05$, whose surface coverage converges to the limit of $\theta = 1$ (see Fig. 2(A)), a_h can be regarded as varying within a small range around 0.65 (red dashed line). Therefore, a consistent fitting parameter of $a_h = 0.65$ used is sufficient to cover most of the simulated systems. When we convert the horizontal coordinate further to $\sigma^{1/3}\ln(1 - a_h\sigma^{2/3})N$ and adopt this constant of $a_h = 0.65$, the values of $\ln(1 - \theta)$ (see Fig. 3(B)) fall roughly on the same linear line (the black dashed line), except for those data points close to the coverage limit.

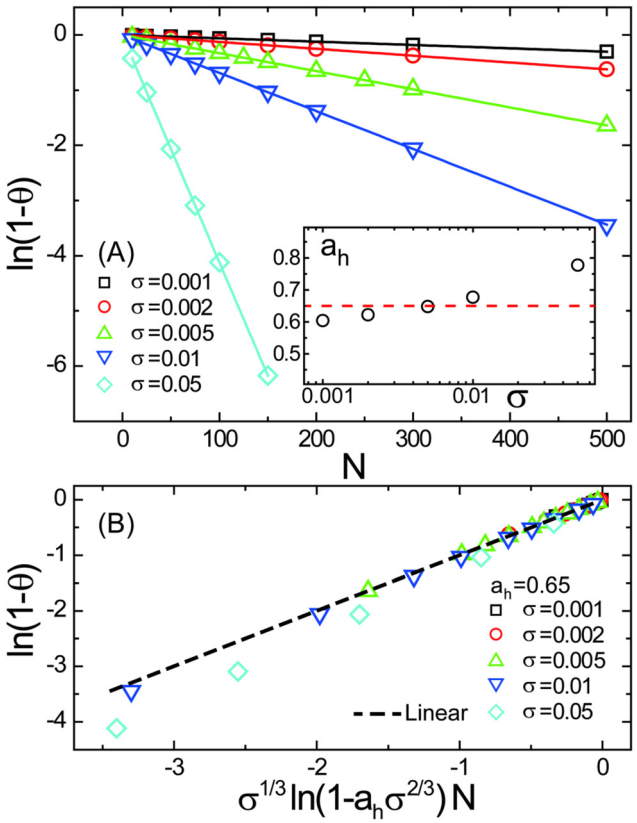

Fig. 3 Rescaled surface coverage $\ln(1-\theta)$ of planar brushes, with different grafting density σ, as a function of the polymer length N. The data points in (A) and (B) are consistent as in Fig. 2(A), except that a different rescaling has been applied to θ and N. Solid lines in (A) represent the linear fitting curves, and the inset displays a_h (the effective projected area of single monomer) calculated from the fitting slopes.

4 Polymers on spherical nanoparticles

4.1 Theoretical analysis

Now, we move from a planar to a spherical substrate and start with polymers in the mushroom state. As shown in Fig. 4(A), a polymer containing N monomers fixed with one end to the spherical NP (with the diameter of D) forms a spherical mushroom of diameter R. The projection area of the single-chain mushroom forms a three-dimensional spherical cap on the NP with the area S_c, height h_c and polar angle ϕ, respectively. The right side of Fig. 4(A) shows the cross section along the centerline of the two spheres, with the edges of the projection determined by the tangent lines from the centre of the NP to the mushroom. Based on the similarity of triangles, we can derive the following equation:

$$\frac{D/2 - h_c}{L\cos\phi} = \frac{D/2}{L}, \tag{13}$$

where L represents the centre-to-centre distance. Therefore, the height of the spherical cap is

$$h_c = \frac{D}{2}(1-\cos\phi), \tag{14}$$

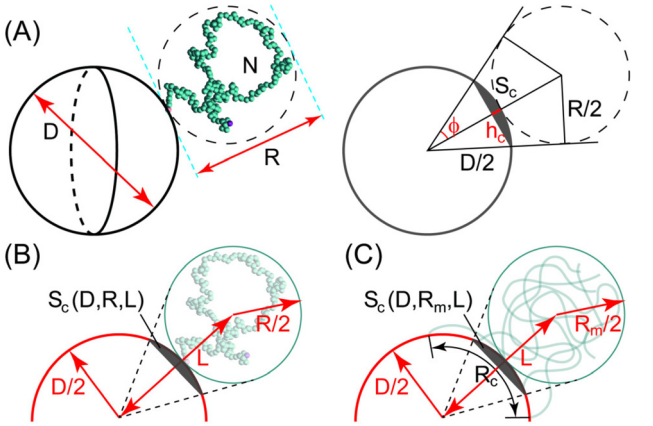

Fig. 4 (A) Schematic illustration of the projected area of a sphere of diameter R on a sphere of diameter D. The black shadow in the right schematic indicates that the projection is a three-dimensional spherical cap with the area S_c, height h_c and polar angle ϕ, respectively. (B) and (C) illustrate the mushroom and micelle morphology of polymers on the NP, respectively, where the black region represents the projection area S_c from the single-chain mushroom or the multi-chain micelle.

yielding the projection area

$$S_c = \pi D h_c = \frac{\pi D^2}{2}(1-\cos\phi), \tag{15}$$

where

$$\phi \equiv \arcsin\frac{R}{2L},\ 0 \le \phi \le \frac{\pi}{2}. \tag{16}$$

Therefore, the projection area of the single-chain mushroom is related to the diameter of the NP (D), the diameter of the mushroom (R) and their center-to-center distance (L), which can be expressed as

$$S_c(D,R,L) = \frac{\pi D^2}{2}\left[1-\sqrt{1-\left(\frac{R}{2L}\right)^2}\right]. \tag{17}$$

For the case of the mushroom being tangent to the NP as shown in Fig. 4(B), $L = (D+R)/2$. We can still define θ using the simplified eqn (7) by substituting the projected area of the mushroom as $S_j = S_c(D,R,(D+R)/2)$.

In good solvent and near the dilute limit ($c \to 0$),

$$\theta \approx \sigma S_c\left(D,R,\frac{D+R}{2}\right)\frac{N}{R^2},\ R = \alpha N^{3/5}, \tag{18}$$

where $(1-c)^R \approx Rc \approx N/R^2$ is used in applying eqn (7). Due to the complexity of calculating S_c, it is not possible to capture the behavior of θ in terms of a simple power law of N. However, we can fit θ *vs.* N numerically, *i.e.*, by using α as a free fit parameter. Here, we make a crude approximation that the effective single monomer projection (set to 1) and the number density of monomers ($c = N/R^3$) remain constant regardless of the distance from the NP. Those assumptions made for the spherical substrate are failing as the limit of $c \to 0$ no longer holds.

For isotropic semi-dilute spherical brushes, we split the radial thickness H into a number of $n = H/l$ spherical shells (see Fig. 1(B)). The shell at a distance r from the centre of the NP contains $\approx 4\pi r^2 c(r) l$ monomers, and the projected area of each monomer (with the diameter of d) in this shell is $a_i = S_c(D,d,r)$. By employing the monomer density derived from the Daoud–Cotton model,[24] *i.e.*, $c(r) = \beta\sigma^{2/3} r^{-4/3}$, the eqn (5) provides

$$\theta = 1 - \prod_{i=1}^{n}\left[1 - \beta\frac{4l(\sigma r)^{2/3}}{D^2} S_c(D,d,r)\right], \qquad (19)$$

where $r \equiv (D+d)/2 + (i-1)l$, β serves as the free fit parameter and H is identified by the boundary condition of $\int_{D/2}^{D/2+H} 4c(r)r^2 \mathrm{d}r = \sigma D^2 N$.

Spherical systems in poor solvent with the condensed limit ($c \rightarrow 1$) can be considered as follows: for polymers in the mushroom state, the surface coverage (eqn (7)) yields

$$\theta \approx \sigma S_c\left(D, R, \frac{D+R}{2}\right), \; R = \gamma N^{1/3}, \qquad (20)$$

where the free parameter γ is used to quantify the size of the single chain patch. Similarly, when polymers form multi-chain micelles tangent to the NP as shown in Fig. 4(C), we substitute the size[25] R_m of a single micelle, which contains $\sim {R_m}^3/N$ chains, in eqn (20). Then, M polymer chains constitute $\sim MN/{R_m}^3$ micelles, yielding a surface coverage of

$$\theta \approx \sigma S_c\left(D, R_m, \frac{D+R_m}{2}\right)\frac{N}{{R_m}^3}, \; R_m = \lambda\sigma^{1/5}N^{3/5}. \qquad (21)$$

We notice that the number of micelles satisfies $\sim \sigma D^2 N/{R_m}^3 \sim D^2\sigma^{2/5}N^{-4/5}$, which is consistent with a previously published model.[26] With the free parameters γ and λ, we can then fit the simulation results of the polymers in the mushroom state and the micelle state, respectively. To ensure physically meaningful results, eqn (18)–(21) must be truncated when $\theta \geq 1$.

4.2 Simulation results

Fig. 5 illustrates the MD simulation results of θ *vs.* N for polymers on a spherical NP. Simulation snapshots corresponding to the data points (labeled (a) to (h)) are shown on the right, where black and cyan beads indicate the NP of diameter $D = 40$ and polymers, respectively. In good solvent (Fig. 5(A)), polymers are either dispersed on the NP in the form of independent chains (snapshots (a) and (e)) or forming a porous semi-dilute brush which dresses the NP. The former case corresponds to dilute chains in the mushroom state, which is well described by eqn (18) (solid lines, $\alpha = 0.85$) at low σ or N. The semi-dilute brushes of higher σ, as described by eqn (19) (dashed lines, $\beta = 85.4$), indicate the formation of the isotropically decorated NP. The transition between these states is shown in the case of $\sigma = 0.005$ (green symbols with green solid and dashed lines).

In poor solvent, polymers undergo a transition from the mushroom state to the micellar state as N or σ increases. Fig. 5(B) exhibits the simulation results over a wide range of

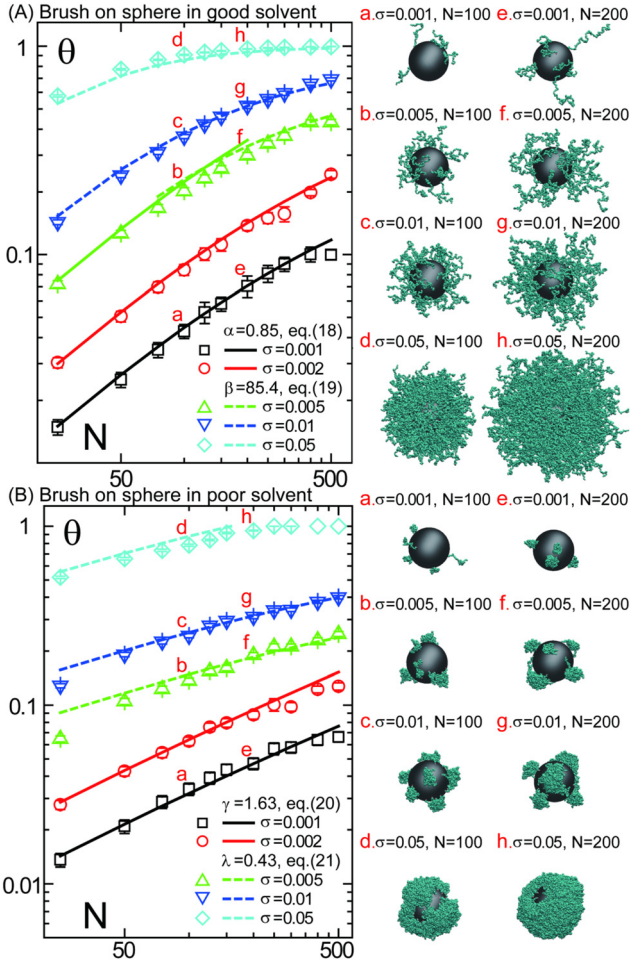

Fig. 5 Surface coverage of spherical substrate θ as a function of polymerization N at various grafting densities. In (A) good solvent, solid and dashed lines indicate the fitted curves of eqn (18) and (19) with the fit parameters $\alpha = 0.85$ and $\beta = 85.4$ (the sublayer thickness is set as $l = 0.1$), respectively. In (B) poor solvent, solid and dashed lines represent the fitted curves of eqn (20) and (21) with the fit parameters $\gamma = 1.63$ and $\lambda = 0.43$, respectively.

coverages θ. Within the range of our simulations ($N < 500$), polymers maintain in the mushroom state when the grafting density is low ($\sigma = 0.001$ and $\sigma = 0.002$, black and red symbols). The fitted curves as obtained from eqn (20) (black and red solid lines) provide a good representation of θ *vs.* N with a constant value of the fit parameter $\gamma = 1.63$. When σ increases (≥ 0.005), we have to apply eqn (21) to fit the simulation data, in which the polymers are predominantly in the micellar state. Similarly, accompanied by a constant fit parameter $\lambda = 0.43$, the data points fall roughly on the fitted curves (dashed lines) at sufficient chain lengths. This good match is maintained up to the limit case at which the NP is fully covered ($\theta = 1$).

In addition, we calculate the difference in surface coverage of spherical substrates (data in Fig. 5) between good and poor solvents, denoted by $\Delta\theta = \theta_{good} - \theta_{poor}$, with respect to grafting density and polymerization as shown in Fig. 6(A). $\Delta\theta > 0$, which is maintained under most conditions, indicates that the polymer coating exposes more area of the NP surface as the

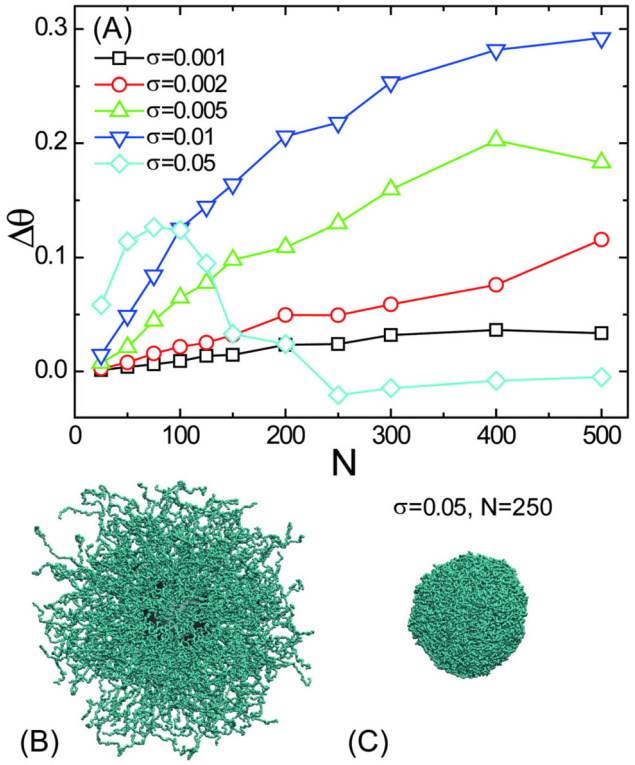

Fig. 6 (A) Difference in surface coverage of spherical substrates in good and poor solvents at the same grafting density and polymerization. $\Delta\theta = \theta_{good} - \theta_{poor}$, where θ_{good} and θ_{poor} are taken from the data in Fig. 5(A) and (B), respectively. Snapshots of spherical brushes with $\sigma = 0.05$, $N = 250$ in (B) good solvent and (C) poor solvent.

solvent quality decreases. This tendency intensifies with increasing σ or N, up to the limit of $\theta = 1$, where $\Delta\theta < 0$ (cyan symbols) may occur under certain conditions. This results from θ reaching its maximum value ($\theta = 1$) in poor solvent, while the porous structure in good solvent leads to slightly lower coverage, yielding negative $\Delta\theta$ values (as shown by the snapshots).

5 Conclusions

In conclusion, using a mean-field and scaling approaches, we derive theoretical models describing the surface coverage of polymers grafted on planar and spherical substrates. The approach covers all general cases of polymers morphologies at different solvent qualities, and its accuracy is verified by MD simulation results. Starting off with planar substrates and then generalizing to spherical substrates, we define coverage and demonstrate how the same can be extracted consistently from molecular simulation data. After a fit procedure which yields constant fit parameters, we obtain semi-quantitative agreement over wide ranges of grafting densities and chain lengths in good as well as poor solvent. Notably, the theoretical framework developed for spherical substrates can be extended to cylindrical systems. The primary distinction arises from the different geometric shapes, which manifest in two key aspects: (1) the calculation of projected area (eqn (17)) and (2) the radial distribution of monomers (incorporated into eqn (19)).

Our work thus provides a novel quantitative tool to analyze the surface properties of polymer-decorated NPs, and to extend the prediction of their properties over wider ranges of system parameters. While experimental analysis does not necessarily require precise knowledge of surface coverage, our work provides essential constraints on experimental parameters when the results are highly sensitive to this quantity. This represents a key contribution of our study, offering guidance for experimental design and interpretation in systems where surface coverage plays a crucial role. Specifically, our theoretical framework enables experimentalists to establish parameter ranges and predict system behavior even when complete microscopic details are not fully characterized.

Among other implications, these findings elucidate how system parameters influence the proportion of exposed substrates that may come into contact with biological or pharmaceutical molecules, providing crucial insights for drug delivery system design and biomolecular interactions. If sufficiently small, these molecules may even diffuse through the porous brush layer onto the substrate. The corresponding penetration probability relates to θ, as quantified in this paper, and plays a key role in the design of polymer-dependent oil/gas transmission[44] and energy storage[45] devices. Apart from that, NPs with 'smart' surfaces have been extensively developed by adopting solvent-stimuli responsive polymers,[46] which vary the surface coverage with the solvent quality. Our model predicts the dependence of the coverage on these system parameters. Taking the blue symbols in Fig. 5 ($\sigma = 0.01$) as an example, for $N = 50$, θ decreases by 20% (0.24 to 0.191) with the switch of the solvent quality from good to poor, whereas this change is enhanced to 34% with longer chains of $N = 100$ (0.369 to 0.244). If we consider the scenario with $N = 500$, θ drops from 0.69 to 0.4, implying that with these parameters we can construct polymer-NP systems in which the NP, originally mostly encapsulated in polymers, exposes 60% of its surface as the solvent deteriorates. Finally, polymer patchy NPs are the most important building blocks of self-assembling structures[4] – the distribution of patches not only affects the kinetic of the assembly, but also its final microstructure. The surface coverage of patches on NP provides clues that, in combination with electron tomography images,[13] allows us to gain complete structural information about the polymer patchy particles.

Author contributions

Cheng-Wu Li: conceptualization, data curation, formal analysis, funding acquisition, methodology, project administration, software, writing – original draft; Holger Merlitz: formal analysis, supervision, validation, writing – review & editing; Jens-Uwe Sommer: supervision, validation, writing – review & editing.

Conflicts of interest

There are no conflicts of interest to declare.

Acknowledgements

This work was supported by the Deutsche Forschungsgemeinschaft (DFG) under grant no. LI 4398/2-1, Project No. 536118308. The authors thank the ZIH of the TU Dresden for providing computational resources.

Notes and references

1 J. Du and R. K. O'Reilly, *Chem. Soc. Rev.*, 2011, **40**, 2402–2416.
2 E. Bianchi, R. Blaak and C. N. Likos, *Phys. Chem. Chem. Phys.*, 2011, **13**, 6397–6410.
3 A. B. Pawar and I. Kretzschmar, *Macromol. Rapid Commun.*, 2010, **31**, 150–168.
4 S. Sacanna and D. J. Pine, *Curr. Opin. Colloid Interface Sci.*, 2011, **16**, 96–105.
5 J.-M. Rabanel, V. Adibnia, S. F. Tehrani, S. Sanche, P. Hildgen, X. Banquy and C. Ramassamy, *Nanoscale*, 2019, **11**, 383–406.
6 M. Yoshida and J. Lahann, *ACS Nano*, 2008, **2**, 1101–1107.
7 S. Ravaine and E. Duguet, *Curr. Opin. Colloid Interface Sci.*, 2017, **30**, 45–53.
8 B. Wang, B. Li, B. Zhao and C. Y. Li, *J. Am. Chem. Soc.*, 2008, **130**, 11594–11595.
9 B. Ebeling and P. Vana, *Macromolecules*, 2013, **46**, 4862–4871.
10 C. Singh, P. K. Ghorai, M. A. Horsch, A. M. Jackson, R. G. Larson, F. Stellacci and S. C. Glotzer, *Phys. Rev. Lett.*, 2007, **99**, 226106.
11 J. Kim, X. Song, A. Kim, B. Luo, J. W. Smith, Z. Ou, Z. Wu and Q. Chen, *Macromol. Rapid Commun.*, 2018, **39**, 1800101.
12 A. M. Percebom, J. J. Giner-Casares, N. Claes, S. Bals, W. Loh and L. M. Liz-Marzán, *Chem. Commun.*, 2016, **52**, 4278–4281.
13 R. M. Choueiri, E. Galati, H. Thérien-Aubin, A. Klinkova, E. M. Larin, A. Querejeta-Fernández, L. Han, H. L. Xin, O. Gang and E. B. Zhulina, *et al.*, *Nature*, 2016, **538**, 79–83.
14 C. Rossner, E. B. Zhulina and E. Kumacheva, *Angew. Chem., Int. Ed.*, 2019, **58**, 9269–9274.
15 M. Yamato, O. H. Kwon, M. Hirose, A. Kikuchi and T. Okano, *J. Biomed. Mater. Res.*, 2001, **55**, 137–140.
16 Y. Wang, Y. Wang, D. R. Breed, V. N. Manoharan, L. Feng, A. D. Hollingsworth, M. Weck and D. J. Pine, *Nature*, 2012, **491**, 51–55.
17 S. C. Glotzer and M. J. Solomon, *Nat. Mater.*, 2007, **6**, 557–562.
18 E. Bianchi, B. Capone, I. Coluzza, L. Rovigatti and P. D. van Oostrum, *Phys. Chem. Chem. Phys.*, 2017, **19**, 19847–19868.
19 O.-A. O. Abiodun, O. Oluwaseun, O. K. Oladayo, O. Abayomi, A. A. George, E. Opatola, R. F. Orah, E. J. Isukuru, I. C. Ede and O. T. Oluwayomi, *et al.*, *Clean Technol.*, 2023, **5**, 934–960.
20 M. Rahmati, E. A. Silva, J. E. Reseland, C. A. Heyward and H. J. Haugen, *Chem. Soc. Rev.*, 2020, **49**, 5178–5224.
21 B. Aveyard, *Surfactants: in solution, at interfaces and in colloidal dispersions*, Oxford University Press, 2019.
22 Q. Yang, M. H. de Vries, F. Picchioni and K. Loos, *Nanoscale*, 2013, **5**, 10420–10427.
23 D. Dukes, Y. Li, S. Lewis, B. Benicewicz, L. Schadler and S. K. Kumar, *Macromolecules*, 2010, **43**, 1564–1570.
24 M. Daoud and J.-P. Cotton, *J. Phys.*, 1982, **43**, 531.
25 D. Williams, *J. Phys. II*, 1993, **3**, 1313–1318.
26 E. Zhulina, T. Birshtein, V. Priamitsyn and L. Klushin, *Macromolecules*, 1995, **28**, 8612–8620.
27 V. Koutsos, E. Van der Vegte, E. Pelletier, A. Stamouli and G. Hadziioannou, *Macromolecules*, 1997, **30**, 4719–4726.
28 B.-C. Choi, S. Choi and D. E. Leckband, *Langmuir*, 2013, **29**, 5841–5850.
29 F. L. Verso, L. Yelash, S. A. Egorov and K. Binder, *Soft Matter*, 2012, **8**, 4185–4196.
30 C. Jentzsch and J.-U. Sommer, *J. Chem. Phys.*, 2014, **141**, 104908.
31 L. Yu, R. Shi, H.-J. Qian and Z.-Y. Lu, *Phys. Chem. Chem. Phys.*, 2019, **21**, 1417–1427.
32 M. Gong, Q. Yu, C. Wang and R. Wang, *Langmuir*, 2019, **35**, 5534–5540.
33 T. Staszewski, *J. Phys. Chem. C*, 2020, **124**, 27118–27129.
34 S. Plimpton, *J. Comput. Phys.*, 1995, **117**, 1.
35 A. P. Thompson, H. M. Aktulga, R. Berger, D. S. Bolintineanu, W. M. Brown, P. S. Crozier, P. J. in't Veld, A. Kohlmeyer, S. G. Moore and T. D. Nguyen, *et al.*, *Comput. Phys. Commun.*, 2022, **271**, 108171.
36 K. Kremer and G. Grest, *J. Chem. Phys.*, 1990, **92**, 5057.
37 G. S. Grest and M. Murat, *Macromolecules*, 1993, **26**, 3108–3117.
38 M. Pütz, K. Kremer and G. S. Grest, *Europhys. Lett.*, 2000, **49**, 735.
39 V. Ahlawat, S. P. S. Deopa and S. Patil, *Nanomaterials*, 2022, **12**, 526.
40 M. Rubinstein and R. H. Colby, *Polymer Physics*, Oxford University Press, New York, 2003.
41 C.-W. Li, H. Merlitz, C.-X. Wu and J.-U. Sommer, *Macromolecules*, 2018, **51**, 6238–6247.
42 S. Alexander, *J. Phys.*, 1977, **38**, 977.
43 P. deGennes, *Macromolecules*, 1980, **13**, 1069.
44 Y. Tsujita, *Prog. Polym. Sci.*, 2003, **28**, 1377–1401.
45 J. Fahlteich, M. Fahland, W. Schönberger and N. Schiller, *Thin Solid Films*, 2009, **517**, 3075–3080.
46 E. Wischerhoff, N. Badi, A. Laschewsky and J.-F. Lutz, *Bioact. Surf.*, 2011, 1–33.

